Ultrasonic Haptic Feedback

6.101 Final Project

Spring 2017

Chris Desnoyers & Sarah Pohorecky

May 18, 2017

Contents

1 Introduction

Ultrasonic haptic feedback uses ultrasound to create a disturbance in the air that the user can feel when they pass their fingertips across it.

Our system contains an array of transducers, each of which transmits a 40 kHz ultrasonic pressure wave. The waves from each transducer are appropriately delayed such that the output waveforms line up at a focal point above the array, making the pressure level (analogous to sound volume) at that point very high (see Fig. 1 for a visualization). In order to reach the greatest possible output power, the transducers need to be driven at approximately 30 VRMS. A 200 Hz signal is modulated onto the ultrasonic carrier and transmitted by the transducers. If the user's finger is placed at the focal point, the skin acts as an envelope detector and a 200 Hz signal is felt as a vibration on the finger (Carter, 2013).

This technology is currently being explored to create novel user interfaces that don't require direct interaction with a surface. For example, in modern vehicles with touch-screen interfaces, tacile feedback using ultrasound could allow the driver to make adjustments without looking at the screen (Ultrahaptics).

For our final project, our goal was to create a phased array of ultrasonic transducers to produce a vibrating midair focal point that a user can feel. To do this, we designed oscillators that provided the 200 Hz and 40 kHz signals, an analog mixer to create the modulated signal, and signal delay lines to provide the proper inputs to each transducer.

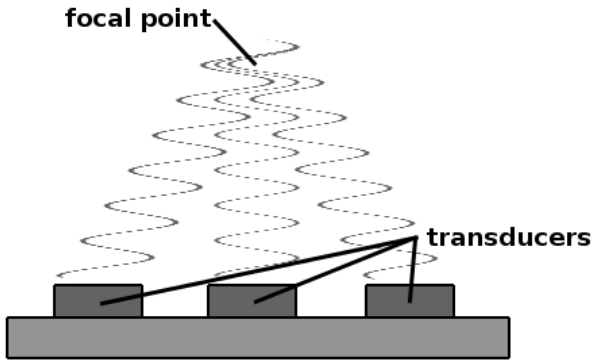

Figure 1: Focal Point Signal Lineup

Additional modules designed for this project were a power supply to provide the 30 VRMS for the transducers, and an signal amplifier/driver for the transducer array. Since the transducers have significant parasitic capacitance that causes poor power usage, the drive circuitry for each transducer provides impedance matching to decrease the amount of current we need to supply from the power supply.

UT-1240K-TT-R 40 kHz piezoelectric transducers were used because of their affordable price point relative to other ultrasonic transducers.

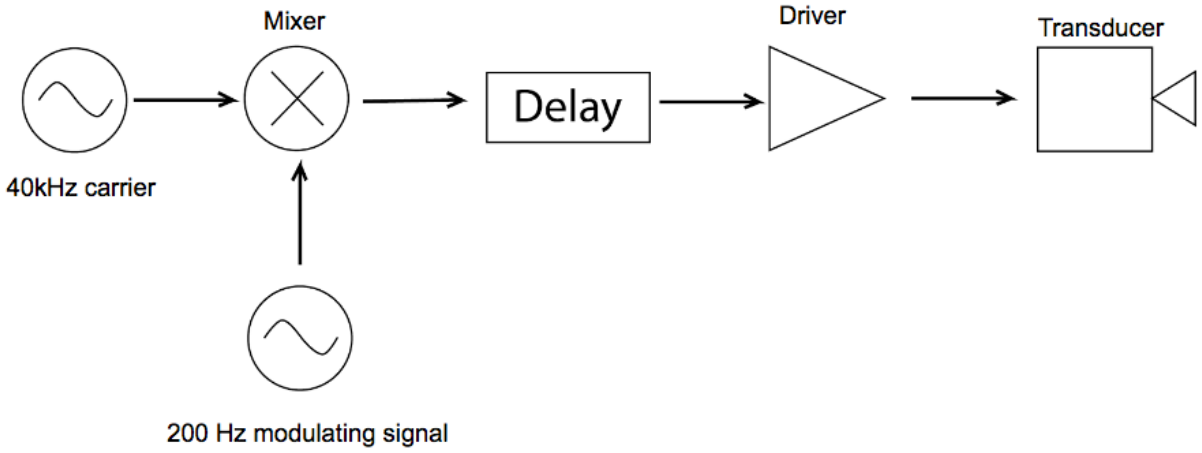

Figure 2: Ultrasonic Haptic Feedback Block Diagram

2 Circuit Design

2.1 Oscillators

Sarah Pohorecky

The transducer signal comprises of a low-frequency signal (200 Hz) modulated onto an

ultrasonic carrier (40 kHz). The oscillators were designed to provide these two signals.

Both oscillators were phase-shift oscillators, which use an RC network to operate an op-amp in unstable mode to create oscillations. See Fig. 3 for schematics. To create unstable operation, the op-amp must have feedback with a 180 degree phase shift from its input. Since the maximum phase shift that can be created from 1 RC pole is 90 degrees, at least 2 poles are required. A solution with 3 poles, each buffered by an additional op-amp to prevent segments from loading each other, creates a very nice sinusoidal oscillation with low distortion and no noise (see Fig. 4). The frequency of oscillation is set by the time constant of the RC network used, such that $f = \dfrac{1}{2\pi \mathrm{RC}}$. The gain and feedback resistors, $\mathrm{R_F}$ and $\mathrm{R_G}$ need to be chosen so that the gain of the circuit, $\dfrac{\mathrm{R_F}}{\mathrm{R_G}} = 8$ to create a gain of 1 at the oscillation frequency (one of the requirements for unstable operation). In practice, this gain sometimes has to be slightly higher to begin oscillation, and has to be adjusted manually. This occurred with our oscillators: while the 40 kHz oscillator used $\mathrm{R_F} = 160$ kΩ and $\mathrm{R_G} = 20$ Ω, with gain of 8, the 200 Hz oscillator required $\mathrm{R_F} = 160$ kΩ and $\mathrm{R_G} = 15$ kΩ with gain of 10.6 before it began to oscillate.

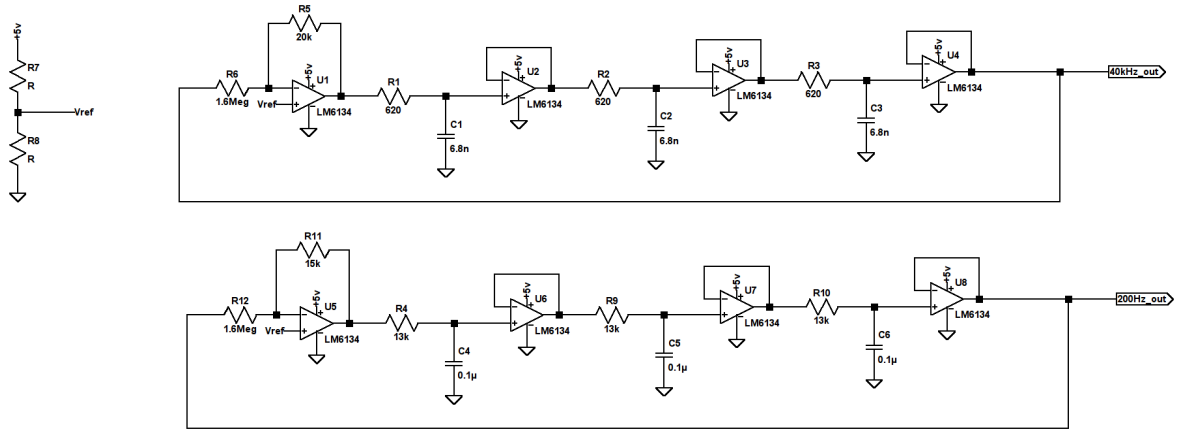

Figure 3: Oscillator Schematics

The 40 kHz oscillator, using 620 Ω resistors and 6.8 nF capacitors, had a calculated frequency of $f = \dfrac{1}{2\pi \times 620\Omega \times 6.8\mathrm{nF}} = 37.7$ kHz, but was measured at a frequency of 41.3 kHz. The 200 Hz oscillator used 13 kΩ resistors and 0.1 μF capacitors, with calculated frequency of $f = \dfrac{1}{2\pi \times 13\mathrm{k}\Omega \times 100\mathrm{nF}} = 122$ Hz and real frequency of 210 Hz.

LM613x op-amps were used for both oscillators. Originally, they were built with LM348s,

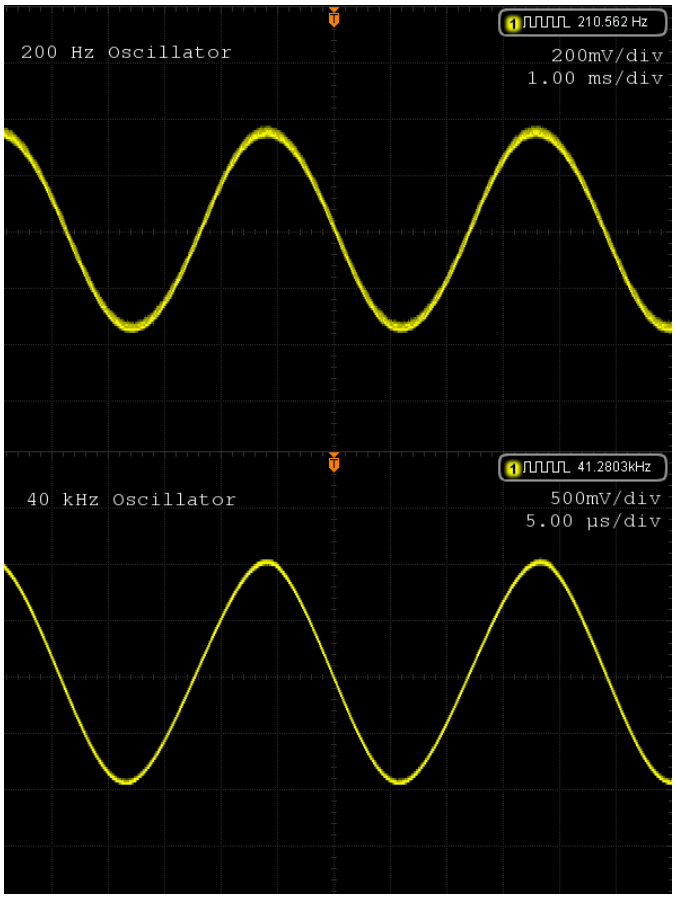

Figure 4: Oscillator Waveforms

but these op-amps proved insufficient for the oscillators, principally due to their low slew rate, which is 0.5 V/μs compared to 14 V/μs for the LM613x op-amps. Originally, we were testing the oscillators for use with a 15 V supply, and with 15 V input, the output waveform was approximately 8 V peak-to-peak. This meant the maximum frequency of oscillation was around 30 kHz, since $8\text{V}/((1/30\text{kHz} * 10^6)/2) = 0.48\text{V}/\mu\text{s}$. While this problem may have resolved with the lower supply voltage of 5 V, the outputs of both oscillators were additionally much more distorted and less clean than the same circuits built with LM613x op-amps, so switching components made sense.

2.2 Mixer

Chris Desnoyers

In order to provide an amplitude-modulated input to the transducer drivers, the outputs of the 200 Hz and 40 kHz oscillators need to be multiplied together. See Fig. 5 for schematics. This is done using a cascode amplifier as a single-quadrant multiplier, in which the 40 kHz carrier is the input to the lower MOSFET and the modulating signal is the input to the upper MOSFET (both are first divided down to be approximately 200 mV pk-pk in

order to keep the mixer within the desired bias region). Biasing is set so that the upper FET is in saturation and the lower FET is in the triode region, resulting in a linear relationship between the carrier gain and the modulating signal level. The output also has a high-amplitude component at the frequency of the modulating signal, which is filtered out by the RC network used for AC-coupling into a common emitter amplifier, which amplifies the modulated carrier. The output of this block is buffered by an emitter follower to allow it to fan out to the analog delays.

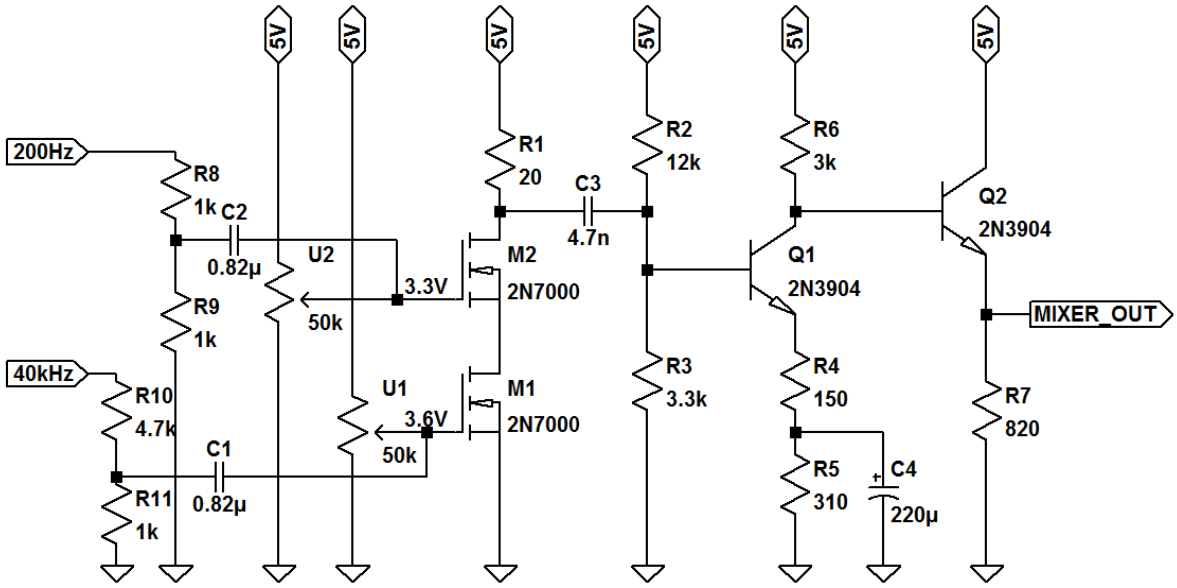

Figure 5: Analog Mixer Schematic

2.3 Analog Delay

Chris Desnoyers

A phased array is focused by applying the proper delay to the signal that is fed to each transducer. These delay circuits are implemented as first-order all-pass filters (see Fig. 6 for schematic), using an RC low-pass filter to introduce phase shift and an op-amp to reverse the attenuation this filter would normally introduce. The following is the transfer function of the filter, where R_{PP} denotes the summed values of the 1 kΩ and 10 kΩ delay potentiometers, and the 5 kΩ potentiometer is set to zero:

$$H(s) = \frac{1 - R_{PP}C_1 s}{1 + R_{PP}C_1 s}$$

The magnitude of the transfer function is unity, and its phase is given by:
$\phi = 2atan(\frac{1}{R_{PP}C_1 2\pi F})$ (Zumbahlen, 2012)

Although the modulated signal has several component frequencies, and a first-order all-pass filter provides a delay that varies with frequency, the component frequencies are clustered so closely around 40 kHz that even in the worst case (90.0 degree phase shift at 40 kHz, which places the steepest phase slope across the signal components) they experience approximately the same delay: 40.2kHz has an 89.7 degree phase shift, 39.8 kHz has a 90.3 degree phase shift, corresponding to ±21 nanosecond range. A 10 kΩ potentiometer provides coarse delay tuning, and a 1 kΩ potentiometer provides fine delay tuning. The delay is determined by the RC constant of the sum of these potentiometer resistances and a 6.8 nF capacitor, providing a delay range from 0.5 μs to 12.5 μs (corresponding to 6.7 to 180 degrees of phase shift on the 40 kHz carrier). This allows the focal point to be moved by computing the necessary delays for each transducer signal, then setting the variable delay potentiometers accordingly.

Focusing a 3x3 transducer array at a point above its center requires the edge transducers to be delayed relative to the corner transducers, and the center transducer to be delayed relative to the edge transducers. The transducers are placed directly adjacent to one another, and have a diameter of 12.8 mm. The transducers have a beam width of 70 degrees, so we chose a focal point 35.7 mm above the center of the array because it is 20 degrees off-center from the edge elements and 27 degrees off-center from the corner elements, less than the 35 at which their output has fallen to half-power, but not so far away that the acoustic power should be significantly reduced by the distance it travels. The necessary delay for each element can be found by dividing the difference of its distance from the focal point and the furthest element's distance from the focal point by the speed of sound in air, 340.3 m/s. For a corner delay of 0 (achieved by bypassing its signal around the delay stage), the edge transducers need a delay of 6.1 μs and the center transducer needs a delay of 12.5 μs.

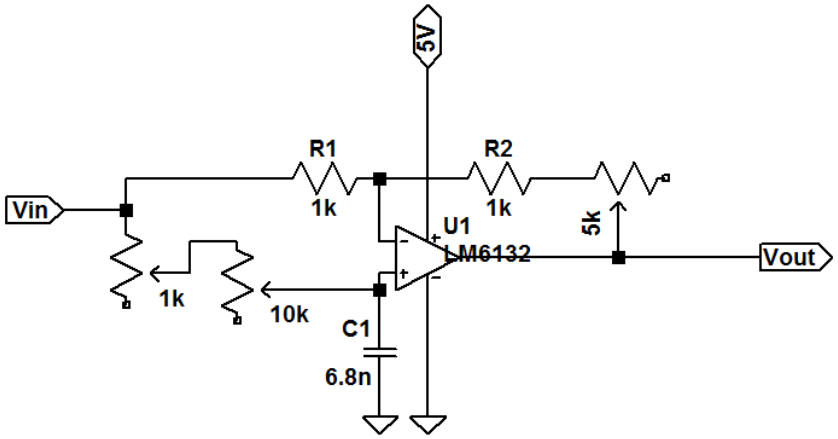

Figure 6: Delay Schematic

A 5 kΩ potentiometer in the feedback network was included in order to provide variable

gain in an earlier incarnation of the circuit, but no longer provides useful functionality in the final version of the design. With this topology, setting the gain potentiometer to a nonzero resistance value to provide greater-than-unity gain changes the transfer function from an all-pass filter to a high-pass filter, as well as altering the phase shift, so the 5 kΩ gain potentiometer can best be considered a mistake and its impact on performance is not represented in the above performance analysis. For completeness, the transfer function including nonzero gain potentiometer resistance (denoted as R_{GP}) is as follows:

$$H(s) = \frac{R_1 - (R_2 + R_{GP})R_{PP}C_1 s}{R_1 + R_1 R_{PP} C_1 s}$$

2.4 Transducer Drivers

Chris Desnoyers

A UT-1240K-TT-R piezoelectric ultrasonic transducer can be approximated by the Butterworth Van-Dyke model, in which the mechanically resonant mode is represented by a series RLC network with the appropriate resonant frequency, and there is a parasitic capacitance in parallel with it (Guan and Liao, 2004). Due to manufacturing variations, the resonant frequency of each transducer, nominally 40 kHz, is actually somewhere between 39 kHz and 41 kHz (PUI Audio, 2016). To simplify the design process, a resonant frequency of 40 kHz was assumed for all transducers, and an impedance analyzer was used to determine an equivalent RC network for the transducer at an operating point of 40 kHz, in which the power dissipation across the resistor approximates the acoustic output power. The datasheet does not provide a full set of modeling parameters, but does provide an estimated value of 2 nF for the parallel capacitance, and a maximum voltage rating of 30 V RMS across the transducer. In practice, the impedance analyzer indicated a capacitance closer to 10 nF for most transducers, with the highest at 90 nF, and an equivalent resistance between 100 Ω and 1 kΩ.

To the best of our understanding, with this model the transducer at 40 kHz acts as a low-pass filter, with the parasitic capacitance preventing the full driver output from being delivered to the load (the resonant leg of the transducer circuit model). Driving a transducer directly from an emitter follower, the only way to get most of our transducers to operate close to full power (as measured in lab) was to use a very small emitter resistor and therefore a very high bias current, dissipating a large amount of power (2.5 W static dissipation for a 500 Ω emitter resistor; 50 mA bias current) across the emitter follower at its bias point. In order to improve efficiency, an LC network was designed to form a parallel-resonant tank with the parasitic capacitance, resonant at 40 kHz, effectively canceling out its undesirable effect on power delivery to the load. Fixed RL622-391K-RC inductors with a nominal value of 390 μH were used, and all were approximately 345 μH at 40 kHz (as measured by an impedance analyzer). An additional parallel capacitance was added and tuned such that the LC network composed of this matching capacitance, the parasitic capacitance, and the matching inductor had a resonant frequency of 40 kHz, at which point it should present a very high impedance to the driver and allow power to be delivered to the lower-impedance series-resonant leg of the transducer. The transducer and matching network were AC-coupled to the driver in order to avoid saturating the inductor with any unintended DC bias at the

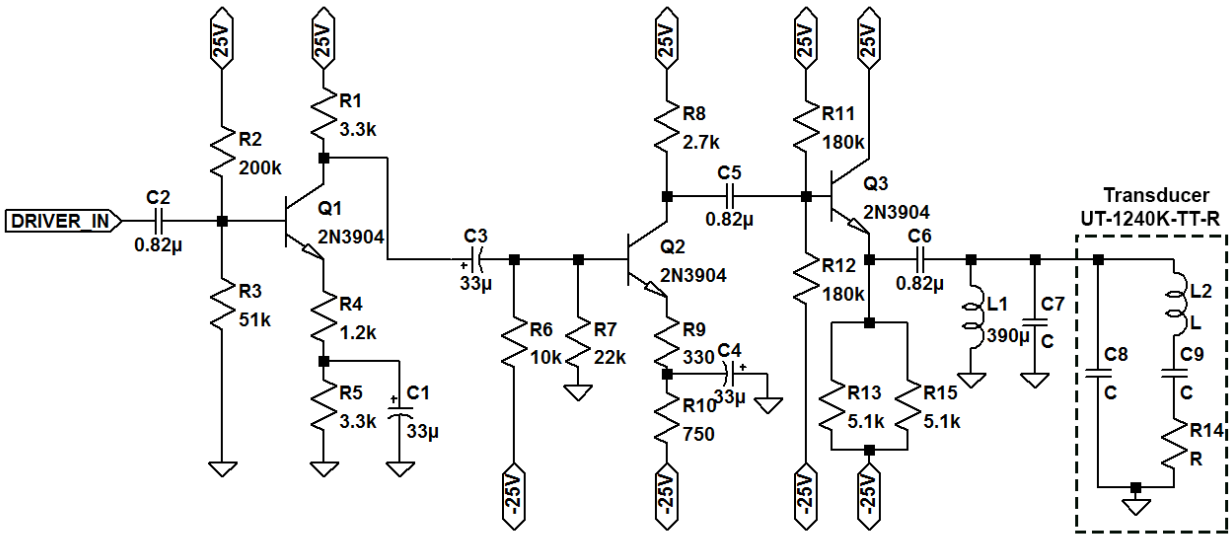

Figure 7: Driver Schematic

output.

See Fig. 7 for the driver schematic. The central stage of the driver consists of a common emitter amplifier with emitter degeneration, which provides gain of approximately 8, and has moderate input and output resistance. This amplifies a 5 V pk-pk sinusoid up to about 40 V pk-pk, close to the transducer's maximum rating of 30 V RMS (42 V pk-pk for a sinusoidal signal). A ±25 V supply provides enough headroom to deliver this output voltage. This gain stage is preced by an additional common emitter amplifier to amplify the delay line output signal from 2.5 V pk-pk to 5 V pk-pk, with a nominal gain of 2.75 but an overall gain of about 2 after accounting for attenuation due to high output resistance on the new stage and low input resistance on the older stage. The driver output is buffered by a common emitter amplifier to reduce the output resistance of the driver, allowing it to drive the relatively low impedance presented by the transducer.

The overall voltage gain, input resistance, and output resistance (prior to the LC matching network) of the driver are approximately as follows (assuming β of 160, a conservative value for the 2N3904 transistors we tested in lab):

$$A_V = \frac{R_1}{R_4} * \frac{R_6||R_7||\beta R_9}{R_1 + (R_6||R_7||\beta R_9)} * \frac{R_8}{R_9} * \frac{R_{11}||R_{12}||(\beta(R_{13}||R_{15}))}{R_8 + R_{11}||R_{12}||(\beta(R_{13}||R_{15}))} = 14.0$$

$$R_{IN} = \beta R_4||R_2||R_3 = 33.5\ k\Omega$$

$$R_{OUT} = \frac{1}{g_{m3}} = \frac{V_{th}(R_{13}||R_{15})}{V_{B3} - V_{BE} + 25V} = 2.6\ \Omega$$

2.5 Power Supply

Sarah Pohorecky

Since the transducers require high-power signals, we designed a step-up power supply to drive the transducer array. The requirements for the supply are that it provide two-rail outputs at +25 V and −25 V respectively, and supply a total of 500 mA, approximately 400 mA at the positive rail, and 100 mA at the negative rail.

The supply topology (see Fig. 8 for the full schematic) was a dual-rail boost converter, which can create both a higher positive voltage and an absolutely higher inverted voltage using one switching signal.

The switching was provided by an N-Channel MOSFET and a 555 Oscillator. The IRF540 was chosen as the switching FET for its power characteristics: $V_{DS,max} = 100$ V; continuous $I_{D,max} = 28$ A; continuous $I_{D,max} = 110$ A. These characteristics were important, as the FET needed to be able to handle the full inductor current as well as the current pulses created by C_2 discharging while on, and the high voltage difference created by the inductor while off.

A boost converter ideally has output $V_{out} = \frac{1}{1-D}V_{in}$ where D is the duty cycle of the switching signal. Since this power supply required a stepped-up voltage of 25 V from 15 V, the ideal duty cycle was 0.4. The switching frequency should ideally be as high as possible, so that the inductor is less likely to fully discharge between cycles (and thus operate discontinuously; a harder-to-analyze mode of operation). The combined rise, fall, and switching delays of the IRF540 is on the order of 100 ns, so a switching signal frequency of roughly 100 kHz was chosen to provide both a large safety margin above the timing constraints of the FET, while being low enough to avoid any concerns about over-clocking the 555.

Since the duty cycle of the switching signal to the boost converter needed to be less than 50%, a slightly different 555 oscillator topology was used, utilizing a diode in series with R_B on the discharge path and another diode bypassing R_B on the charging path to allow the charging and discharging times to be independently adjusted. The frequency of oscillation of this topology is then given by $\frac{1}{C(R_A + R_B)}$ and the duty cycle is given by $\frac{R_A}{R_A + R_B}$.

This oscillator used $R_A = 3.9\text{k}\Omega$, $R_B = 10\text{k}\Omega$ and C= 1 nF. These gave calculated frequency and duty cycle of 71.9 kHz and 28% respectively. The real values of these measurements were 76.3 kHz and 36%.

All diodes used were MUR120s, for their high pulsed voltage and current rating, and all capacitors used were non-polar electrolytics rated for 50 V.

The final design had 13.01W/15.15W = 86% efficiency. (input 15 V at 1.1 A; output 26 V across 68 Ω and −25 V across 220 Ω). Most of this power loss is presumed to have occured across the inductor, as that was the only circuit component (excluding the load resistors) that noticeably increased in temperature during operation (the FET, while certainly dissipating some power, was not warm to the touch).

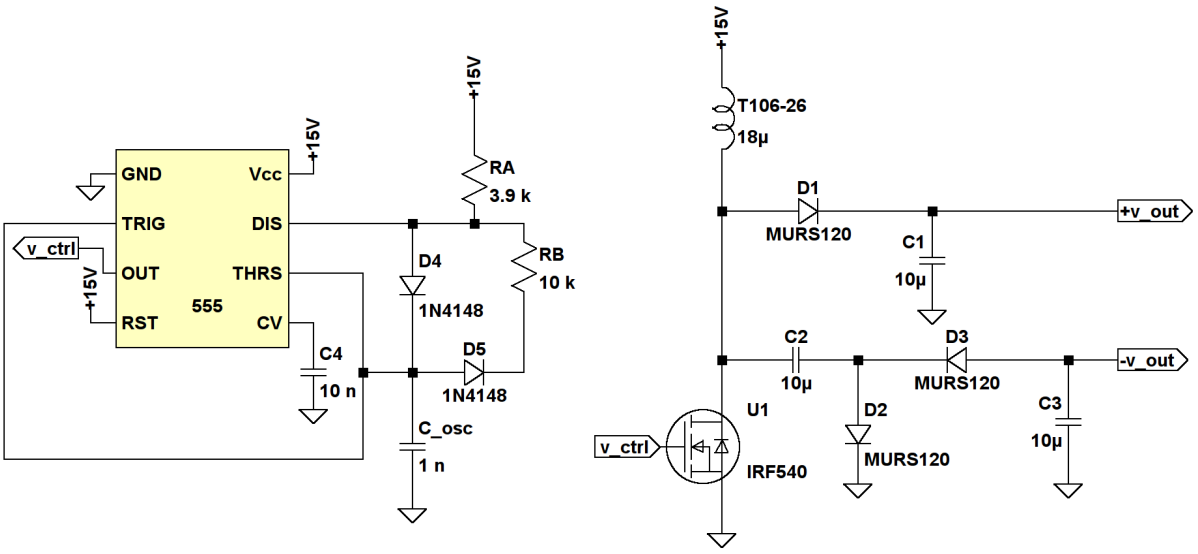

Figure 8: Power Supply Schematic

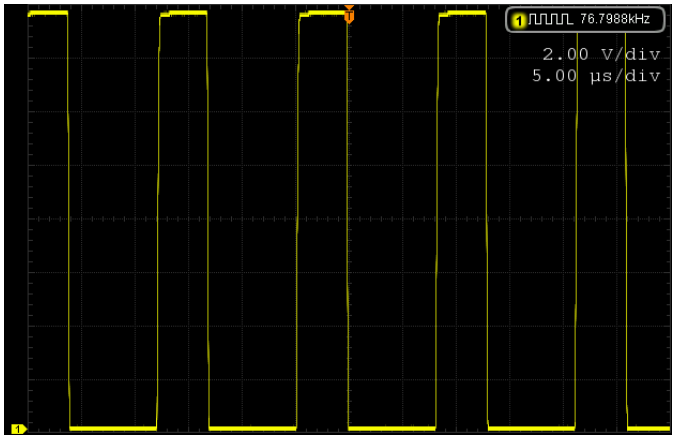

Figure 9: Boost Converter Control Signal

The major problem with this design was the lack of feedback. With anticipated current load (tested with 68 Ω and 220 Ω power resistors on the positive and negative outputs of the boost converter), the converter output was at expected level. However, if the current load was smaller than calculated, the voltage increased at the output and across the inductor. This meant that variable current in our circuit would either over-volt the transducer drivers, or also possibly burn out components of the converter itself (which happened while testing with small current load and the voltage across the inverting capacitor exceeded 50 V).

The solution to this problem is to use feedback from the boost converter output to control the duty cycle of the switching signal. While a basic design for this was created and tested, it did not end up robust enough to inductor noise to use in the final circuit. The basic design

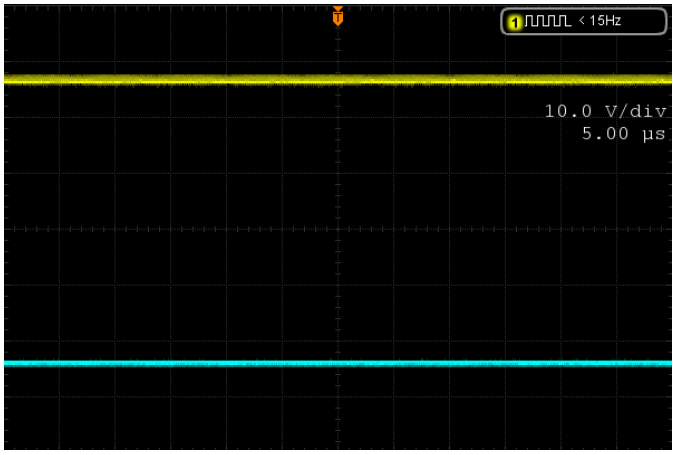

Figure 10: Boost Converter Output

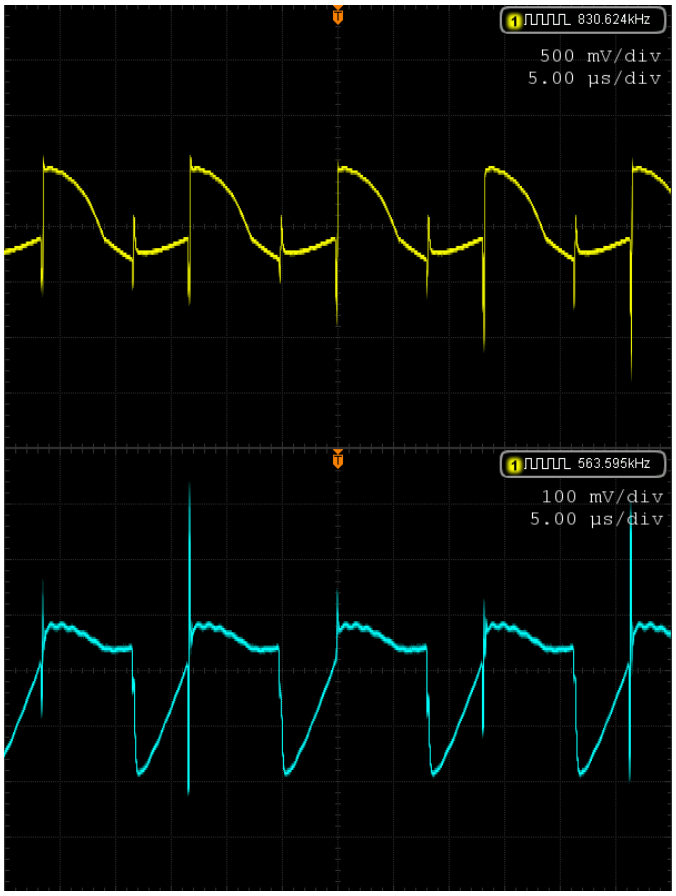

Figure 11: Boost Converter Ripple Voltage (top: positive rail)

was to take the output of the positive rail of the converter, divide it down, and use the divided output and a triangle wave as the inputs into a comparator to generate a variable-duty-cycle square wave. While the comparator circuit worked when tested without the converter, noise

from the inductor in the converter caused significant false triggers on the comparator without the use of hysteresis, and there was not enough time to change the design before the deadline.

3 Results

Our final system was tested with 5 transducers running simultaneously, powered by lab supplies. There was a noticeable, though weak, area of sensation at the focal point which was qualitatively stronger than the sensation produced using a single transducer. This was tested using both the oscillator-mixer-delay input to the array, as well as function generator-delay (where the function generator provided the modulated signal). Both methods produced a tactile sensation, though the function generator produced a sightly stronger output.

The power supply was complete and functional, although was not integrated into the rest of the system due to several problems discussed in the next section.

At the start of the project, we programmed a microcontroller to replace many of the analog signal functions in the event that one of our subsystems didn't work, but in the end, we did not need it, as we completed every required module and implemented the full system in analog.

4 Challenges

Our final deliverable worked, although it was not as complete as we had planned. We encountered a number of challenges with various modules and integration.

The first of the challenges we encountered, as was mentioned earlier, was the lack of robustness with our power supply. Since the supply did not include any feedback control, with loads smaller than our estimated current draw (which we believe in hindsight may have been higher than in reality), the voltage at both rails would increase and cause problems both in the supply and in the rest of the circuit. In the end, we did not test our system with the boost converter supply, and instead used lab power supplies, as we were worried about accidentally burning out the rest of our system. While a feedback system was designed, there was no hysteresis in the comparator circuit of the original design and the output signal had many false triggers caused by interference from the rest of the converter and was not acceptable for controlling the converter. A redesign of the feedback system using a more robust comparator circuit with hysteresis would have solved this problem by eliminating the false triggers.

In the mixer stage, variation in the output amplitude due to variation in the power supply voltage between different bench supplies was also a challenge, one that was addressed with the inelegant solution of introducing variable gain in the delay stage, which interfered with the desired operation of the delay stage (see Section 2.3). A source degeneration resistor from the lower MOSFET to ground would improve mixer bias stability in the face of variations

in MOSFET charcteristics and power supply voltage, and therefore might be an alternative solution to the problem of variable output amplitude, but it was not immediately clear how to resolve this solution with the original biasing scheme, so it was only ever explored in simulation.

Another unexpected issue we encountered was the variability of individual transducers. We were aware from the beginning of the project that in order to increase the efficiency of driving our transducer array, we would have to build a matching network to compensate for parasitics in the transducers, but we were not expecting the large variability in individual transducers that we found existed in reality. This meant that each individual transducer had to be compensated for individually, eating up time we had expected to dedicate to other parts of the project.

Another driver issue was inductor saturation. Although we could not tell for certain whether or not this was happening, using 500 mA-rated inductors opened up the possibility that the inductors may have been saturating and operating at a lower effective inductance than expected. Measurements taken on one driver indicated that this was most likely not the case, but some odd behavior at the output (briefly exhibiting a more perfectly sinusoidal shape before settling to a less perfectly sinusoidal shape of lower amplitude) seemed like it could be explained by inductor saturation.

Finally, we failed to plan for the amount of time it would take to build multiple copies of our circuit designs. We had at one point hoped to drive sets of transducers on a common delay with a single driver, requiring only 3 working drivers to test array focusing at a fixed point above the center of the array, but the variation in transducer characteristics made this infeasible, as multiple transducers on a single driver would be driven so unevenly that it is likely only one or two would produce the desired level of acoustic power. For the full array, we would have needed 9 separate drivers, which required more time than we had remaining as we approached the end of the project. Thus, our final system was tested with only 5 of our transducers, as we only had time to build 5 drivers, and even these 5 were not tuned as well as we would have liked.

5 Conclusion

While we encountered a number of challenges, and our system was not as robust as we had hoped, our final design was a fully analog system that created a tactile sensation in midair.

Considering that our final test was with only five out of nine transducers, but produced a stronger sensation than a single transducer, we believe that we could have attained a stronger sensation with the full three-by-three array. Performance additionally could have been improved with more precise tuning of the drivers to each of the transducers.

6 Bibliography

Abdel-Rahman, Sam, Franz Stuckler, and Ken Siu. "PFC Boost Converter Design Guide." *Infineon.* February 22 2016. Web.
http://www.infineon.com/dgdl/Infineon-ApplicationNote_PFCCCMBoostConverterDesignGuide-AN-v02_00-EN.pdf?fileId=5546d4624a56eed8014a62c75a923b05

Carter, Tom, et. al. "UltraHaptics: Multi-Point Mid-Air Haptic Feedback for Touch Surfaces." *UIST '13, ACM.* October 8-11, 2013. Web. http://dl.acm.org/citation.cfm?id=2502018

Coates, Eric. "Wien Bridge Oscillators." *www.learnabout-electronics.org.* Web. http://www.learnabout-electronics.org/Oscillators/osc34.php

De Stasi, Frank. "Working with Boost Converters." *Texas Instruments, Application Report.* June 2015. Web. http://www.ti.com/lit/an/snva731/snva731.pdf

Fan, Haifeng. "Design tips for an efficient non-inverting buck-boost converter." *Analog Applications Journal.* Q3 2014. Web. http://www.ti.com/lit/an/slyt584/slyt584.pdf

Garcia-Rodriguez, M. et al. "Low Cost Matching Network for Ultrasonic Transducers." *Physics Procedia 3.* 2010. Web.

Guan, Mingjie and Wei-Hsin Liao. "Studies on the Circuit Models of Piezoelectric Ceramics." *Proceedings of 2004 International Conference on Information Acquisition.* 2004. Web.

Kim, Jima et. al. "Electrical Modeling of Piezoelectric Ceramics for Analysis and Evaluation of Sensory Systems." *IEEE Sensors Applications Symposium.* 2008. Web.

Kollman, Robert. "Power Tip 60: Three simple split-rail power supply topologies." *EE Times.* June 06 2013. Web. http://www.eetimes.com/author.asp?section_id=183&doc_id=1280919&page_number=1

Lundberg, Kent. "Become One with the Transistor." Version 3.3. 2007. Print.

Mancini, Ron. "Design of op amp sine wave oscillators." *Analog Applications Journal. Texas Instruments Incorporated.* August 2000. Web. http://www.ti.com/lit/an/slyt164/slyt164.pdf

Mancini, Ron and Richard Palmer. "Sine-Wave Oscillator." *Texas Instruments, Application Report.* March 2001. Web. http://www.ti.com/lit/an/sloa060/sloa060.pdf

Mancini, Ron and Richard Palmer. "Sine-Wave Oscillator." *Texas Instruments, Application Report.* March 2001. Web. http://www.ti.com/lit/an/sloa060/sloa060.pdf

Niknejad, Ali. "BJT/FET Mixers/Mixer Noise." *UC Berkeley EECS 142.* 2005. Web. http://rfic.eecs.berkeley.edu/~niknejad/ee142_fa05lects/pdf/lect17.pdf

PUI Audio. "Ultrasonic Transmitter Datasheet." *PUI Audio.* 2016. Web. http://www.mouser.com/ds/2/334/UT-1240K-TT-R-957964.pdf

Ultrahaptics. "Ultrahaptic Applications." *Ultrahaptics.* Web. https://www.ultrahaptics.com/applications/

Zumbahlen, Hank. "Allpass Filters." *Analog Devices.* 2012. Web. http://www.analog.com/media/en/training-seminars/tutorials/MT-202.pdf